Open access e-Journal
Earth Science India eISSN: 0974 – 8350
13 (3), 2020, 78-95
http://www.earthscienceindia.info/

Neoarchean A-Type Granite in the Bundelkhand Craton near Kuraicha: Implications for Crustal Reworking

Mir Md Ramiz[1], M.E.A. Mondal[*] and Iftikhar Ahmad
Department of Geology, Aligarh Muslim University, Aligarh-202002, India
[1]Present address: National Mineral Development Corporation Limited,
Bacheli Complex, Chhattisgarh- 494553, India
*Email: erfan.mondal@gmail.com

ABSTRACT

A distinct Neoarchaean granite is identified from the Bundelkhand Craton in Kuraicha area, Jhansi district, Uttar Pradesh. These granites are fine to medium grained, metaluminous to peraluminous in nature, enriched in silica and K, and very low in FeO^t+MgO+MnO, Ni, Cr, V concentration. They show pronounced negative Eu-anomaly, HREE enriched patterns and very low Sr/Y ratio. They show A-type characters and plot in the A2 field with high Y/Nb ratio. High ZST of 684-799ºC along with increasing Rb/Sr for decreasing Ba concentration in the Kuraicha granites indicate high temperature melting in a fluid absent condition at shallow crustal depths. We propose this A-type granite are the product of high temperature re-melting of older crust and mark the culmination of granite magmatism in the Bundelkhand Craton and thus represent a phase of major tectonothermal reworking event during the Neoarchean.

Keywords: Bundelkhand Craton, granites, A-type, reworking, Neoarchean

INTRODUCTION

The Archean Eon of the Earth's history is marked by high heat production and accretion rates that favored some typical petrogenetic association such as ultramafic komatiitic rocks in the greenstone terranes and voluminous TTG (tonalite, trondhjemite and granodiorite) magmas (Martin *et al.,* 2005). As time progressed, there was a considerable decrease in the TTG production leading to the onset of generation of more potassic and less sodic granitoids during Neoarchean (Laurent *et al.,* 2014; Shirey and Hanson, 1984; Smithies, 2000).This transition between production of high sodic TTG rocks and medium- to high-K granitoids during the Neoarchean remains a matter of debate (Champion and Sheraton, 1997; Frost *et al.,* 2006; Mikkola *et al.,* 2011; Moyen *et al.,* 2003).The petrogenesis of Paleo- to Mesoarchean TTG gneisses is ubiquitous and has attracted the focus of large number of workers in understanding the Archean crustal evolution (Barker, 1979; Barker and Arth, 1976; Martin *et al.,* 2005; Martin and Moyen, 2002; Moyen, 2011; Moyen and Martin, 2012). But, the genesis and evolution of Meso- to Neoarchean voluminous granitoids which include sanukitoids and the high-K granitoids demand more understanding in spite of the considerable work that has already been done. The diversity in these granitic rocks suggests involvement of different sources and/or different depths of melting for their genesis.

Please cite this article as*: Ramiz, Mir Md, Mondal, M.E.A. and Ahmad, Iftikhar (2020) Neoarchean A-type granite in the Bundelkhand Craton near Kuraicha: Implications for crustal reworking. Earth Science India, v. 13 (3), pp. 78-95. https://doi.org/10.31870/ESI.13.3.2020.7*

These granitoids hold the key to record the various crust forming processes throughout the geological time especially during the Neoarchean. Often, an episode of juvenile crust formation is followed shortly by crustal reworking (Hill, 1993; Rey *et al.,* 2003). Crustal reworking is especially considered important in stabilization of the craton and determining their final composition. Crust derived A-type granites highlight a special case of crustal reworking, because of the high temperature magmas from which it crystallizes, is comparatively higher than other intracrustal granites (Creaser *et al.,* 1991; King *et al.,* 2001). Understanding the petrogenesis of such granites is very useful in understanding the crustal evolution of a cratonic block (Bonin, 2007; Frost and Frost, 2011). These crust derived A-type granites originate from a number of sources and hence understanding their petrogenesis is crucial in tracking complex cratonic evolutionary history.

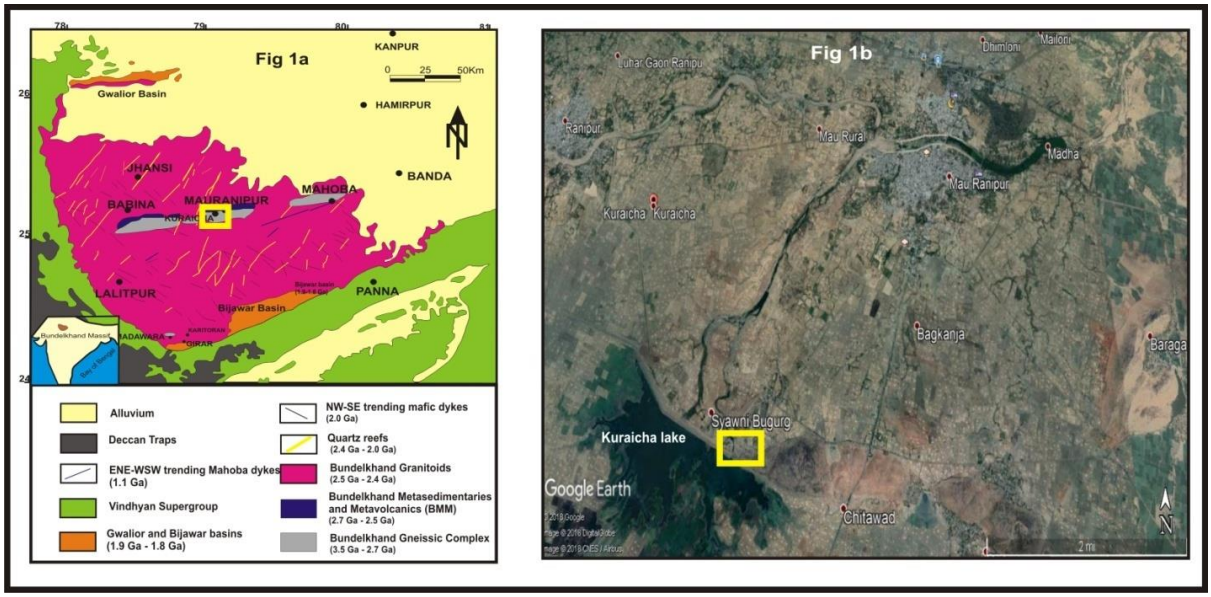

Fig. 1. (a) Generalized geological map of the Bundelkhand Craton (BkC) showing different lithounits (after Basu, 1986). Inset shows the position of the massif in the Indian shield. (b) Satellite imagery taken with the help of Google Earth shows the location of the outcrop with respect to Mauranipur and Kuraicha villages. The yellow boxes in both the figures show the studied area.

The Bundelkhand Craton (BkC) is one such older continental nuclei preserved in the Indian shield with the oldest rock dating back to 3.55 Ga. Like most of the Archean cratons, the main architecture of the continental crust of the Bundelkhand Craton, are the sodic granitoids mainly tonalite-trondjhemite-granodiorite (TTG) rocks, granodiorites and high-K granitoids which make up more than eighty percent of the total crust. Previous studies suggested that the granitic crust formation in BkC took place in the order of hornblende granitoids, biotite granitoids and leucogranitoids in a subduction setting (Mondal and Zainuddin, 1997). The leucogranitoids are considered to represent the youngest phase of granitic magmatism which formed with the least contribution from mafic melt. They are also considered as a marker of culmination of granitic magmatism during Neoarchean-Paleoproterozoic in the BkC. The study of these granitoids were refined lately on the basis of geochemical studies as HSLM (High Silica Low Magnesia) granitoids including monzogranites and LSHM (Low Silica High Magnesia) granitoids including sanukitoids and Closepet-type granitoids (Joshi *et al.,* 2017). There is a consensus regarding their genesis in a subduction zone setting in Neoarchean (Mondal *et al.,* 2002; Joshi *et al.,* 2017; Kaur *et al.,* 2016; Verma *et al.,* 2015). Several pulses of granitoid magmatism occurred between 2.57 to

2.49 Ga (Joshi *et al.,* 2017; Kaur *et al.,* 2016) in the BkC and these granitoids are geochemically distinguished but geodynamically clubbed in same category *i.e.* subduction related. Although many studies are carried out on the nature of granitoid magmatism of the BkC, several issues related to the culmination and stabilization of the craton remains enigmatic. Granitoids show great diversity in their origin and nature and can be formed from a variety of sources in numerous tectonic settings and thus are good petrogenetic indicators. One such distinct variety of granitoids is identified for the first time with the occurrence of heavy rare earth element (HREE)-enriched A-type granitoids from the Kuraicha area of the BkC (Fig. 1a). This is very uncommon, considering the fact that a vast study on the Bundelkhand granitoids has already been carried out in the past by number of workers (Joshi *et al.,* 2017; Kaur *et al.,* 2016; Mondal and Zainuddin, 1997; Singh *et al.,* 2020). The petrogenesis and role of these distinct granites in the crustal evolution of BkC have remained enigmatic. The current study examines integrated field, petrography, and new whole rock major and trace element data including published data of the granitoids from the Kuraicha area of the BkC to explain their genesis in a new perspective.

GEOLOGICAL SETTING OF THE AREA

The BkC lies at the heart of the Indian shield and forms a semicircular massif. It covers an area of about 26000 $Km^2$and is principally composed of Archean granite-gneiss bodies. In the west it is separated from the Aravalli Craton by the NE-SW trending Great Boundary Fault; in the north lies the Indo-Gangetic alluvium; in south and southeast it is delimited by the Son Narmada Lineament; and in the southwestern part some small outcrops of Deccan basalt are present. Besides these, the BkC is overlain by the arcuate shaped Mesoproterozoic Vindhyan basin in the south and southeastern section. Major lithology of BkC includes the grey colored Paleo- to Mesoarchean TTG gneisses which are best exposed in the central parts of the craton *(Kaur et al., 2014; Mohan et al., 2012; Mondal et al.,* 2002; Saha *et al.,* 2016). These TTG gneisses intruded by the younger undeformed granitoids form the basement of the BkC (Basu, 1986). The other components of the basement complex include the Bundelkhand metasediments and metavolcanics (BMM) which occur along two E-W trending lineaments, one in the central part namely the Central Greenstone Belt (Malviya *et al.,* 2006; Verma *et al.,* 2016) and the other in the south i.e. the Southern Greenstone Belt near Girar (Singh and Slabunov, 2015); the Madawara Ultramafic Complex (Singh *et al.,* 2010; Ramiz *et al.,* 2018) and the Neoarchean undeformed intrusive granitoids (Joshi *et al.,* 2017; Kaur *et al.,* 2016; Mondal *et al.,* 2002; Verma *et al.,* 2016). The Neoarchean felsic magmatism in the BkC represents a major geological event which occurred on a large scale marking the stabilization of the craton (Mondal *et al.,* 2002). The successive events of granitoid magmatism took place between 2.57-2.49 Ga (Joshi *et al.*, 2017; Mondal *et al.,* 2002). Besides these, other major lithology in the region consists of the NW-SE trending mafic dykes and the NNE-SSW and NE-SW trending giant quartz veins (Pati *et al.*, 2008, 2007; Pradhan *et al.,* 2012) (Fig. 1a).

STUDY AREA AND SAMPLING

The study area is represented by an outcrop of pink granite situated at the eastern side of the abutment of the Kamla Sagar dam in Kuraicha village, SE of Mauranipur (GPS: 25º12’625” N, 79º06’087” E). The position of the outcrop with respect to Mauranipur is shown with the help of satellite image (Fig. 1b). Close-up view of the same outcrop near the eastern abutment of the dam is shown with a zoomed in Google Earth image (Fig. 2). The outcrop is a medium to fine grained pink colored granitic hillock which is stacked with a number of joint sets. It contains xenoliths of highly deformed and migmatised gneiss (Fig. 3a), indicating the gneiss to be the older crust. Fresh samples of granitoids were collected from the central portion of the hillock. Rocks with alteration and sites of intense deformation were avoided. Sample No. KH449, KH450, MR150(G) and MR155(G) were collected from the above depicted outcrop (Fig. 3 a, b). We have also compared our data with similar rock

(Kaur *et al.,* 2016). Geochemical data of available one TTG sample (BK7) of the Kuraicha gneiss is also reproduced for comparison (Kaur *et al.,* 2014).

Fig. 2: Zoomed-in satellite view taken with the help of Google Earth showing location of the outcrop at the eastern side of the abutment of Kamla Sagar dam in Kuraicha.

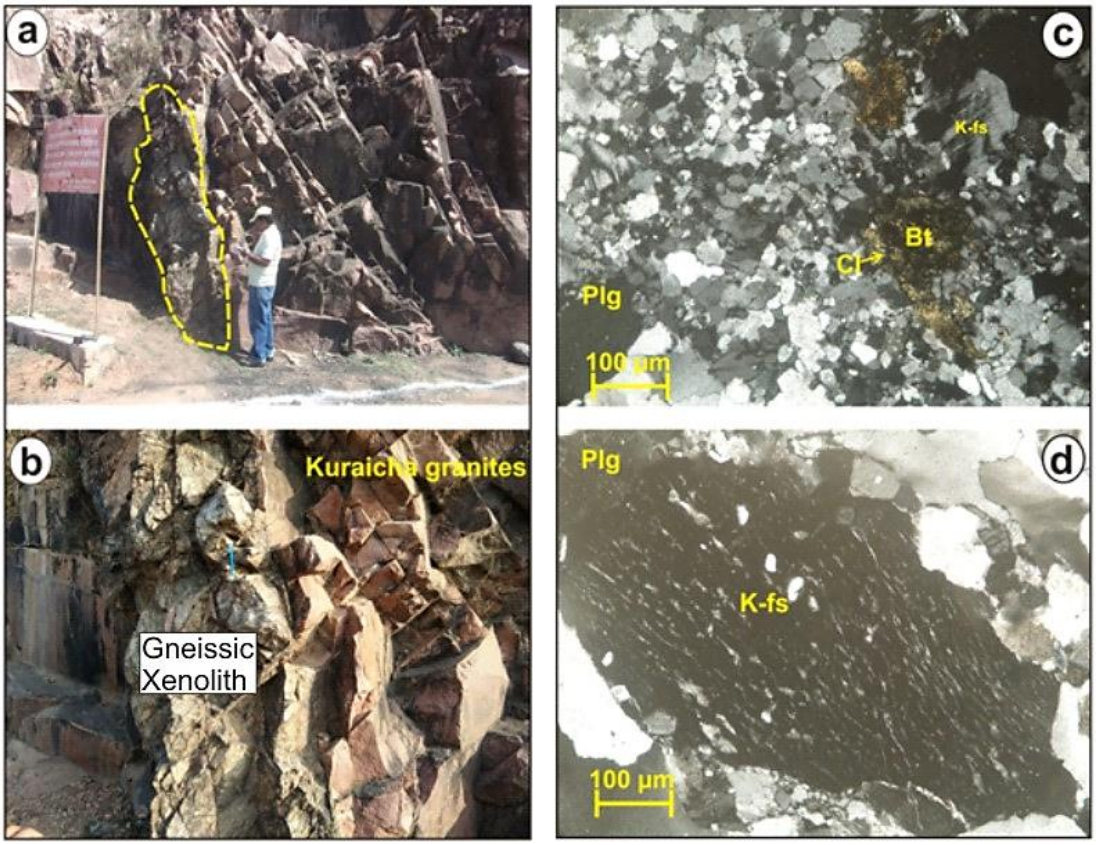

Fig. 3: (a) Photograph showing gneiss (in dotted lines) caught up in the fine-medium grained pink granites near Kamla Sagar dam, Kuraicha. (b) Close-up view of the gneissic xenolith within the granite. Note the gneiss is migmatised and granite is fine-medium grained. (c) Photomicrograph showing fine grained quartz and plagioclase; biotite grains are chloritised at the rims. (d) Photomicrograph showing perthite as a major textural attribute in the Kuraicha granites which resulted due to the late stage fluid released by the biotite breakdown. Plg, Plagioclase; K-fls, K-feldspar; Bt, Biotite; Cl, Chlorite.

PETROGRAPHY

Major mineral assemblage of the Kuraicha granites consists of quartz, plagioclase, K-feldspar (generally microcline), with or without secondary chlorite after biotite; magnetite, apatite, titanite and zircon are found as accessory phases. Quartz and plagioclase are the most abundant minerals followed by the K-feldspar. Biotite is the main mafic mineral present (less than 5 vol%) which are replaced by chlorites in some of the samples (Fig. 3c). Overall, mafic minerals are very less in quantity (less than 8 vol% modally). Both coarse grained and fine grained quartz are seen under the microscope. Perthite texture in the plagioclase grains highlights the role of K-metasomatism in the granites due to the late stage fluids released from the biotite breakdown during melting (Fig. 3d). Based on the mineral mode, the studied granite samples are plotted in QAP classification diagram (Streckeisen, 1976) and they fall in the monzo-granite field (Fig. 4a). This is also supported by the normative An-Ab-Or ternary diagram (Fig. 4b). Kaur et al. (2016) reported that the sample BK-9 (sampled from Kuraicha and used in discussion) display moderate to well-developed foliation.

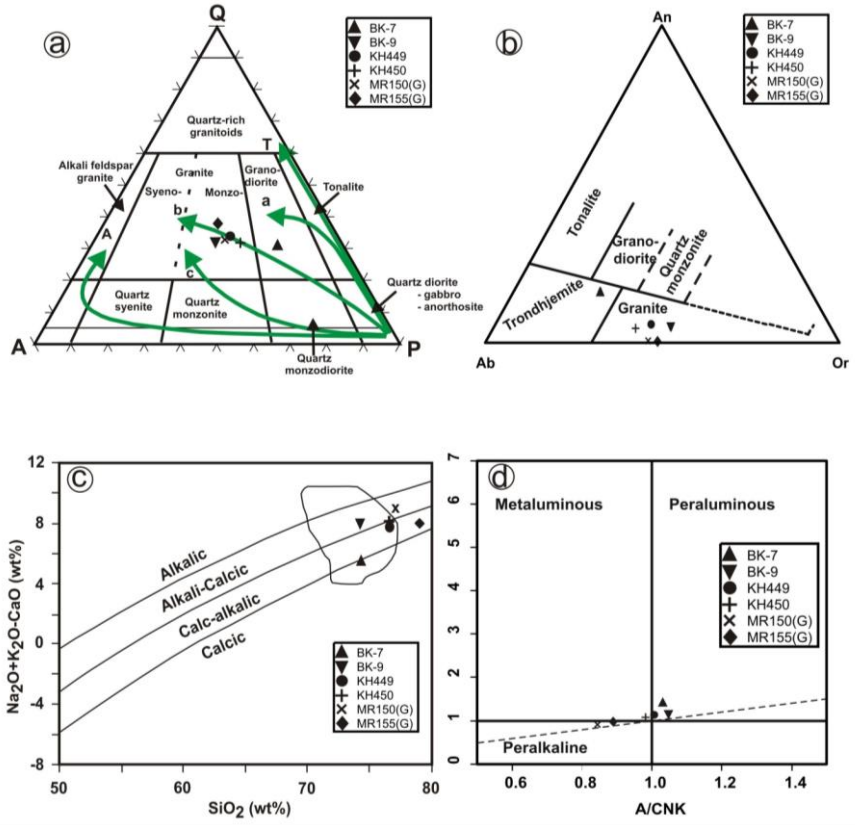

Fig. 4: (a) Modal compositions of the Kuraicha granites along with BK9 and BK7 from Kaur *et al.* (2016) in the QAP classification diagram of Streckeisen (1976). Arrow refers to trend of various plutonic suites after Lameyre and Bowden (1982). A: alkaline suite, T: tholeiitic suite and the calc-alkaline suites include, a: K-poor, b: intermediate and c: K-rich. (b) CIPW

normative An-Ab-Or triangular diagram of O'connor (1965) (fields after Barker, 1979) showing all the Kuraicha granites plot in the granite field. (c) MALI vs SiO_2 diagram for Kuraicha granites, field denotes peraluminous leucogranites of Frost *et al.* (2001) (d) A/NK vs A/CNK diagram of Shand (1943) showing slight metaluminous to peraluminous character for Kuraicha granites.

ANALYTICAL TECHNIQUE

Four samples KH449, KH450, MR150(G) and MR155(G) were analyzed for their whole rock major and trace elements with the analytical procedure for MR150(G) and MR(155G) already provided (Ramiz and Mondal, 2017). The analytical protocol for samples BK7 and BK9 is also provided (Kaur *et al.,* 2016, 2014). For rest of the samples major elements have been analyzed by X-Ray Fluorescence Sequential Spectrometer (XRF-Siemens SRS-3000) at the Wadia Institute of Himalayan Geology (WIHG), Dehradun while trace elements have been analyzed using high resolution inductively coupled mass spectrometer (HR-ICP-MS; Nu Instruments Attom, UK) at the CSIR-National Geophysical Research Institute (NGRI), Hyderabad. Pressed pellets were prepared for major element analysis by XRF following the established protocol. For trace element analysis, 50 mg of the homogenized sample powder was digested using strong mineral acids, the details of which are given elsewhere (Satyanarayanan *et al.,* 2014). International rock standard reference material JG-1A (JGS) and G-2 (USGS) were used for calibration and calculation of precision and accuracy of the samples. The average accuracy and precision of the major element XRF data is ±1% RSD, while the accuracy and precision achieved for the HR-ICP-MS trace element analysis is better than 4% RSD. Geochemical data of the Kuraicha granites are presented in Table-1.

GEOCHEMISTRY

The Kuraicha granites show geochemical characteristics similar to that of the late-Archean biotite granites and HSLM (high silica low magnesian) granites of Joshi et al. (2017), *i.e.* high SiO_2 contents (74.3-79.17 wt%) and high K_2O contents (4.54-5.34 wt%) indicating their highly evolved nature. The MgO content is very low (0.05-0.66 wt%). Al_2O_3 content is much lower (avg. = 12.4 wt%) compared to the gneisses (BK7 =15.02 wt%). The Kuraicha granites have high alkali contents (avg. Na_2O+K_2O= 8.88 wt%) and K_2O/Na_2O ratio in the range of 1.04 to 1.58 (greater than 0.5) indicating its potassic nature (Moyen, 2011). All the samples mostly range from calc-alkalic to alkali-calcic in the modified alkali-lime index (MALI) versus SiO_2 diagram (Fig. 4c) and fall in the peraluminous leucogranite field of Frost *et al.* (2001).

The chondrite normalized rare earth element (REE) patterns of the Kuraicha granites are unique and uncommon as compared to other granites reported so far from the BkC. Earlier studies reveal that REE patterns of the granites are moderately to highly fractionated with $(La/Yb)_N$= 9.8 – 35.4. But in our study we found that our samples show relatively flat REE patterns with enriched HREE patterns with $(La/Yb)_N$ = 0.49 to 2.23, whereas the sample BK9 shows $(La/Yb)_N$= 9.82 (Kaur *et al.,* 2016) (Fig. 5). The HREE enrichment in our sample is also evident by the $(Gd/Yb)_N$ ratios that range from 0.29 to 0.55 except in BK9 which is 1.54. All the samples exhibit very strong negative Eu-anomalies (Eu/Eu* = 0.07-0.31). Total REE concentration is considerably lower (∑REE = 51.7 – 117 ppm) than the earlier reported data on granites; BK9 having ∑REE concentration of 278 ppm. In the primitive mantle-normalized multi-element diagram, large ion lithophile elements (LILE) show enrichment with respect to high field strength elements (HFSE); however, the enrichment is not as pronounced as observed in other Neoarchean granitoids reported elsewhere. The Kuraicha granites are characterized by positive peaks of Rb, Th, U and Pb along with negative troughs of Ba, Nb-Ta, Sr and Ti (Fig.5.) indicating dominant role of crustal melts.

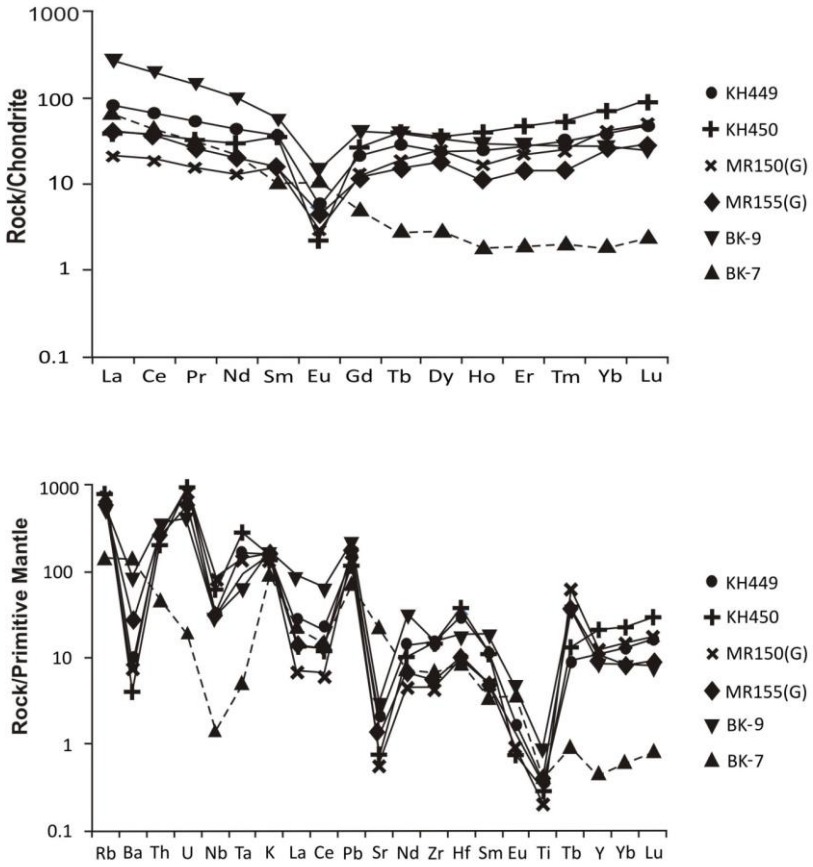

Fig. 5: (a) Chondrite-normalized rare earth element (REE) patterns for the Kuraicha granites and gneiss. Kuraicha granites show considerable HREE enrichment, sharp negative Eu anomalies. On the other hand, Kuraicha gneiss show highly fractionated pattern and HREE depleted patterns. Chondrite values are taken from McDonough and Sun (1995). (b) Primitive mantle-normalized multi-element diagram for the Kuraicha granites and gneiss. Enrichment of K, Rb, Th, U, Pb and negative troughs of Ba, Sr, Nb, Ti indicates crustal signatures. Primitive mantle elemental values are taken from Sun and McDonough (1989). Solid lines are used for granites and dotted line is used for gneiss. Symbols used are same as in Fig. 4.

DISCUSSION

The Kuraicha granites are mainly granites (*sensu stricto*) in terms of both mode and normative composition (Fig. 4a, b). Almost all the studied samples are metaluminous to peraluminous, with one sample being slightly peralkaline in nature (Fig. 4d). Absence of ferromagnesian minerals like amphiboles and pyroxenes in the granite samples and their peraluminous nature along with high silica content and calc-alkalic to alkali-calcic nature point towards their derivation from crust without any significant contribution from mantle. This is also reflected by their low FeO^t+MgO+MnO concentration (avg 1.17 wt%) and low TiO_2, Ni, Cr and V content (Table-1). All these characteristics point towards the A-type nature of Kuraicha granites (Bonin, 2007; Creaser *et al.,* 1991; Frost and Frost, 2011). Various discrimination diagrams are used to discriminate A-type granites from other varieties of granites (Pearce *et al.,* 1984; Whalen *et al.,* 1987).The tectonic discrimination diagram show that the Kuraicha granites fall in the within-plate granites (WPG) field, whereas the gneissic sample BK7 (Kaur *et al.,* 2014) fall in the volcanic arc granite (VAG) field (Fig. 6) *(Pearce et*

al., 1984). This may represent formation of these granitoids in post-collisional environments. Caution should be used in using the conventional tectonic discrimination diagrams of Pearce *et al.* (1984) as they were recently evaluated by Verma *et al.* (2012) based on parameters derived from major elements and immobile trace elements. This suggested that the conventional tectonic discrimination diagrams (Pearce *et al.,* 1984) are less suitable for depicting collision tectonics. In the present study, the number of granitoid samples is inadequate to decipher the tectonic setting more precisely using the discrminant function-based multidimensional tectonic diagrams of Verma *et al.* (2012). This is pressing to note that the geochemical signatures of the granitoids are indicative of their source rock and do not confine them to a particular tectonic environment (Pearce *et al.,* 1984).The Kuraicha granites with high 1000*Ga/Al (> 2.6) and elevated HFSE contents fall in the "A-type fields", whereas the gneissic sample BK7 fall in the "I- and S- type field" (Fig. 7).

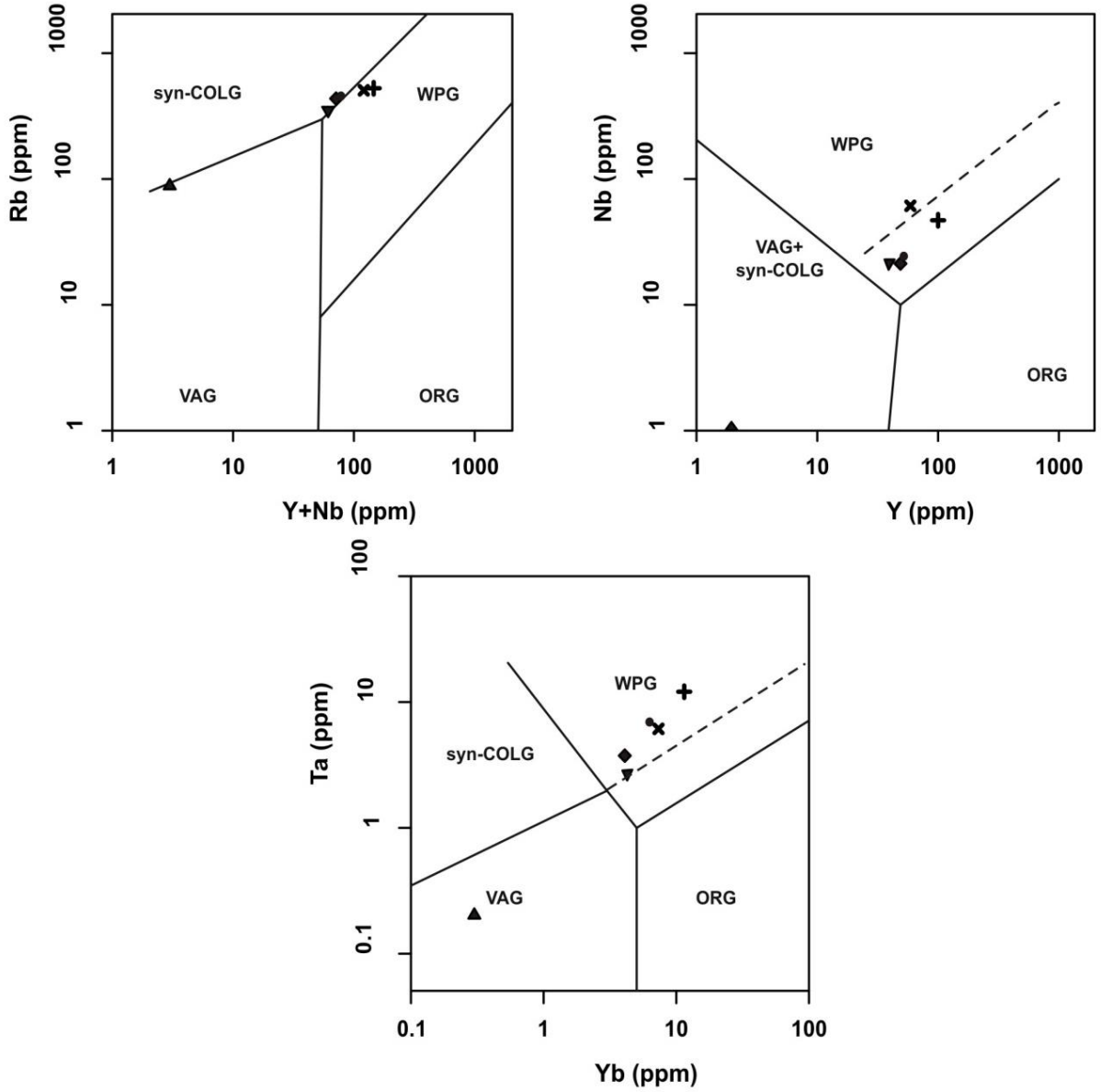

Fig. 6: Tectonic discrimination diagram (Pearce *et al.,* 1984) for Kuraicha granites. The granite samples plot in the WPG fields whereas, the gneissic sample BK7 fall in the VAG field. VAG, Volcanic Arc Granites; synCOLG, Collisional granites; WPG, Within plate granites; ORG, Ocean ridge granites. Symbols used are same as in Fig. 4.

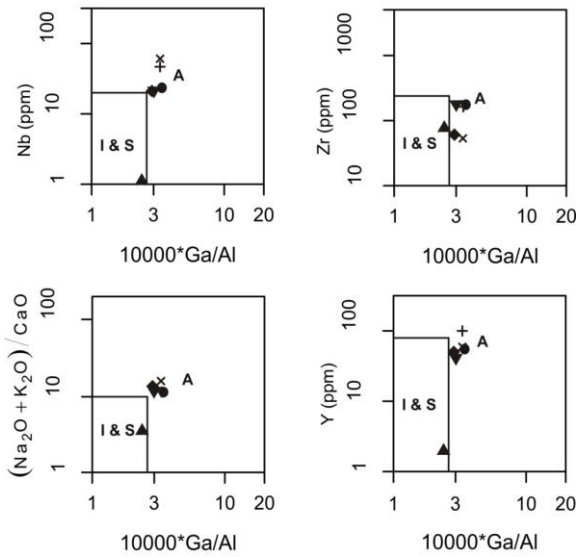

Fig. 7: Plotting of the Kuraicha granites and gneiss (data from Kaur *et al.,* 2016, 2014)) on the classification diagram of Whalen *et al.* (1987)showing A-type affinity for Kuraicha granites and gneissic sample plot in the I- and S-type field. Symbols used are same as in Fig. 4.

Like other granitoids, A-type granitoids also have diverse sources for their origin. The A-type granitoids are classified into two subclasses: A1 and A2 (Eby, 1992). According to Eby (1992), the A1 group is characterized by element ratio similar to those observed for oceanic–island basalts. They represent differentiates of magmas derived from oceanic-island basalts but emplaced in continental rift settings during intraplate magmatism, whereas, the A2 group represents magmas derived from continental crust or underplated crust that has undergone a cycle of continent-continent collision or island arc magmtism. One of the criteria for this division is the Y/Nb ratio. The Kuraicha granites, with high Y/Nb ratios (> 1.2 except one sample) plot in the A2 field (Fig.8). Various petrogenetic processes have been proposed for the generation of A-type granitoids including partial melting of tonalitic to granodioritic, amphibolitic, charnockitic to felsic granulitic source rocks (Du *et al.,* 2016; Gorring *et al.,* 2004; King *et al.,* 2001).

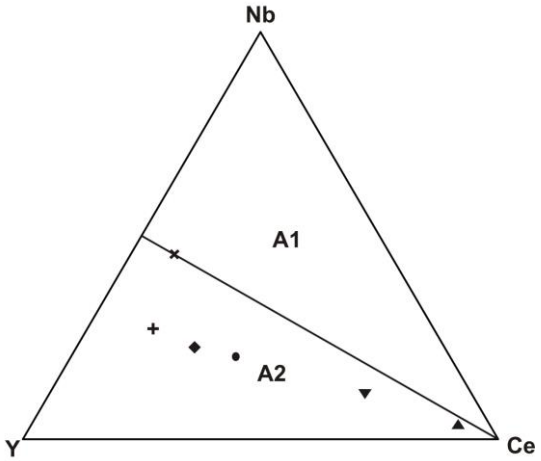

Fig. 8: Kuraicha granites fall in the A2 type field of Nb-Y-Ce triangular diagram of Eby (1992).

Frost and Frost (2011) divided A-type granitoids into eight subclasses on the basis of major element compositions with each class being related to different sources and petrogenetic processes. According to that scheme, Kuraicha granites are classified as metalauminous to peraluminous, calc-alkali to alkali-calcic, which generally forms by the partial melting of the crust. In addition, the samples show Ce/Pb and Nb/U ratios quite similar to the Upper Continental Crust (UCC) (Taylor and McLennan, 1985) and Bulk Continental Crust (BCC) (Rudnick and Fountain, 1995) in the plots of Guo and Wilson (2012), indicating major role of crustal melt in their genesis (Fig. 9). Crustal signatures are also strengthened by the enrichment of Rb, U, Th, Pb, K. The Kuraicha granites have high LILE/HFSE ratios and conspicuous negative Nb, Sr and Ti- anomalies. These signatures in the Kuraicha granites indicate that it has resulted from reworking of a proto-crust (gneissic crust). The probable source candidates include the older gneisses of the Bundelkhnad Craton.

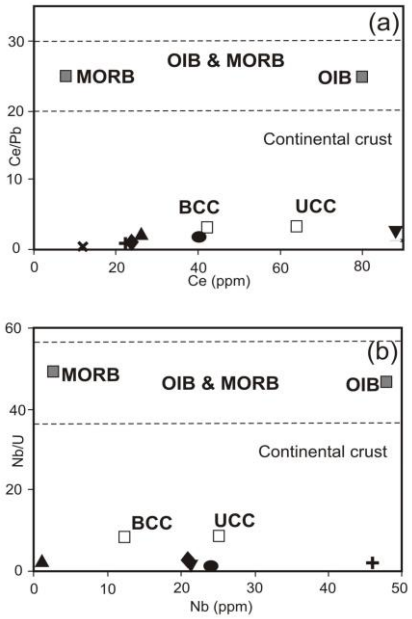

Fig. 9: (a) Ce/Pb versus Ce and (b) Nb/U versus Nb plots (after Guo and Wilson, 2012)). Data for MORB and OIB(Sun and McDonough, 1989); upper continental crust (UCC) Taylor and McLennan 1985), and bulk continental crust (BCC) (Rudnick and Fountain, 1995). Ce/Pb and Nb/U ratios of Kuraicha granites close to UCC and BCC imply them to be crustal melts. Symbols used are same as in Fig. 4.

Plagioclase and garnet are two minerals whose stability and abundance is extremely pressure-dependent and they play key role in controlling the concentration of important trace elements during the partial melting of plagioclase and amphibole bearing rocks (Moyen and Stevens, 2006; Moyen *et al.,* 2009). Plagioclase is stable at 10 kb and generally disappears at pressure excess of 10 kb depending on the temperature and source composition. It also controls the concentration of Sr and Eu (magnitude of Eu anomaly) in the melt. Generally, melts coexisting with plagioclase are relatively Sr and Eu poor owing to higher K_D (partition coefficient) of plagioclase in these elements. In the chondrite-normalized REE diagrams (Fig. 5a) there are sharp negative Eu anomalies in the Kuraicha granite samples pointing towards greater plagioclase retention in the source which is quite common in the upper crustal depths. In addition, the Sr depletion in the primitive mantle normalized multi-element diagram (Fig. 5b) also strengthens that plagioclase was a residual phase. Garnet on the other hand is a high pressure mineral (greater than 12 kb) and becomes abundant with increasing pressure. It controls the concentration of HREE and Y in the melt (Moyen and

Stevens, 2006; Moyen *et al.,* 2009). HREE enrichment is consistent in both chondrite-normalized REE as well as primitive mantle-normalized multi-element diagrams along with lower $(La/Yb)_N$ and $(Gd/Yb)_N$ ratios (table 1) that suggest the Kuraicha granites are formed leaving behind no residual garnet in the source. Flat REEs with HREE enrichment, strong negative Eu anomalies (Eu/Eu* = 0.07-0.31) and Sr anomalies indicate that the Kuraicha granites are result of melting of crustal rocks at a very shallow depth where plagioclase was stable and no residual garnet was present in the source.

Watson and Harrison (1983) established the following relation among zircon solubility, temperature and major element composition of the melt :

$$\ln D^{Zr,\ zircon/melt} = \{-3.8 - [0.85\ (M - 1)]\} + 12900/T$$

where $D^{Zr,\ zircon/melt}$ is the Zr concentration in zircon (~476 000 ppm) to that in the saturated melt, M is a compositional factor that accounts for dependence of zircon solubility on SiO_2 and peraluminosity of the melt [(Na+K+2Ca)/(Al*Si)] (all in cation fraction); and temperature *T* is in Kelvin which is converted in ºC in the paper. Rearranging the above equation, *T* yields a geothermometer for the melt:

$$T_{Zr} = 12900/[2.95 + 0.85M + \ln(496\ 000/Zr_{melt})]$$

The zircon saturation temperature (ZST) for Kuraicha granites ranges from 684-799 ºC suggesting high melting temperatures (Table-1) (Fig. 10a). High temperatures are warranted to melt crustal rocks. Crust derived melts are generally the products of incongruent melting of micas (generally muscovites) as they provide low temperature conditions at which melts can be produced from crustal source in fluid/water absent conditions (Harris *et al.,* 1995). Breakdown of amphiboles and biotites is facilitated in fluid absent conditions. Experimental studies have shown that in fluid present melting conditions, biotite stability is maximum (Scaillet *et al.,* 1995). In Fig. 10b, increasing Rb/Sr for decreasing values of Ba in the Kuraicha granites imply dehydration melting (breakdown) of the micas and amphiboles in the gneisses in fluid absent condition. This trend is attributed to the low melt fraction with restitic K-feldspar because of low degrees of partial melting resulting in increase in Rb/Sr ratio and the partition coefficient of K-feldspar for Ba is high (Inger and Harris, 1993). The increase in Rb and decrease in the Ba content can also be seen in the primitive mantle-normalized multi-element diagram.

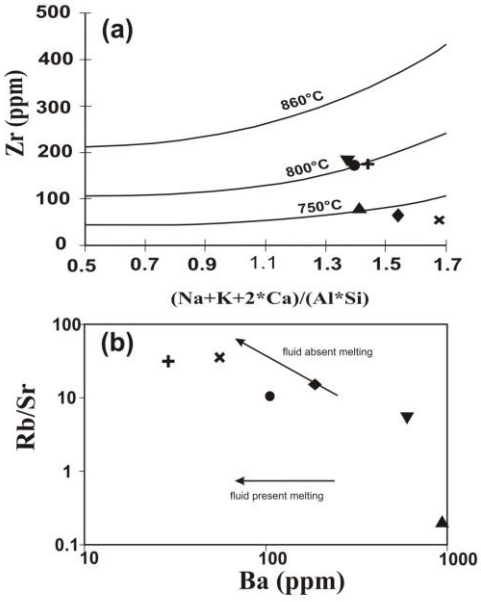

Fig. 10: (a) Whole rock Zr (ppm) vs. (Na+K+2*Ca)/(Si*Al) (cation ratio) diagram with experimentally determined crystallization temperature curves (Watson and Harrison, 1983)) showing high temperature ranges for Kuraicha granites and gneiss. (b) Rb/Sr versus Ba plot for Kuraicha granites and gneiss. Fluid-present and fluid-absent melting trends are from Inger and Harris (1993). Kuraicha granites follow the fluid-absent melting trend. Symbols used are same as in Fig. 4.

Fig. 11: Photograph showing swarms of mafic magmatic enclaves (MMEs) in the ~2.5 Ga Bundelkhand granitoids near Orccha are semi-contemporaneous (Ramiz and Mondal, 2017). The abundance of MME confirms the role of mafic magma in generating high heat for melting of older crust.

IMPLICATIONS ON NEOARCHEAN CRUSTAL EVOLUTION

The sample BK9 yields a concordia age of 2545±10 Ma (Kaur *et al.,* 2016). The Kuraicha granites, therefore represent the final episode of a poorly recognized but one of the significant tectonothermal event. The granites exhibit A2 type nature, which are the characteristics of post-orogenic granites. Post-orogenic granites generally are emplaced shortly after the period of orogensis (Eby, 1992) which in our case is represented by ~2.5 Ga granitoid magmatism in BkC. Lack of well constrained geochemical as well as the geochronological data is proved to be a major handicap in delineating these granitoids. It is proposed that such A-type granite magmatism should not be localized in and around Kuraicha only, but it should have spread all over the batholiths. The available age data of the Kuraicha granites represents one of the important phase of this major tectonothermal event as these granitoids are the result of a post-collisional or post-tectonic setting which usually, but not always, have a gap of 10-20 million years after compressional tectonism (Eby, 1992).

Rey *et al.* (2003) postulated a number of mechanism which include occurrence of mantle plume, thermal blanketing by greenstone volcanic belts, crustal thickening and hot subduction or a combination of these for the reworking of continental crust in Archean. A-type granites are the product of crystallization from high temperatures (Creaser *et al.,* 1991; King *et al.,* 2001). In order to melt crustal rocks, an external heat source is required which is capable of raising the crustal temperature substantially. Coeval mafic magmatism can account for formation of such granites (Creaser *et al.,* 1991; Du *et al.,* 2016). Evidence for coeval mafic magmatism with the Bundelkhand granitoids comes from the recent studies by Ramiz and Mondal (2017). They reported that the mafic magmatic enclaves (MMEs) which

are very common in the Bundelkhand granitoids were semi-contemporaneous (Mondal *et al.,* 2002) with the granitoid emplacement and resulted due to the rapid cooling of the mafic magma inside a cooler acidic magma chamber (Fig. 11). This mafic magma provided ample heat to the crust that led to the crustal-reworking and regeneration of the high temperature A2 type granitic magma. WPG signatures of the granites, corroborates our proposition that the Kuraicha granites formed as a result of incongruent melting of the older gneissic crust. The unmelted migmatised caught up fragment of the older gneiss within the pink granites near Kamla Sagar dam is one of the robust evidence of our proposition (Fig. 3a and b). Occurrence of caught up gneiss within these granites, their fine to medium grained texture and different geochemistry from rest of the granitoids of BkC have great implications for study of Neoarchean crustal evolution as the Kuraicha granite type of rocks represents the culmination phase of the granitic magmatism in the BkC. Similar granitic phase has been reported from Singhbhum craton recently (Topno *et al.,* 2018). This suggests similar tectonic processes were active during the Neoarchean.

CONCLUSION

The Kuraicha granites of the BkC are fine to medium grained and distinct from rest of the granitoids in the region. The studied outcrop is seen having a sharp contact with a caught up gneissic xenolith. Geochemical studies of these granites reveal that they are high-silica, K-rich, calc-alkalic to alkali-calcic and metaluminous to peraluminous rocks. These granites exhibit features of A2 type of granites. They have very low MgO, Mg#, Ni, Cr, V, pronounced negative Eu-anomaly, HREE enriched pattern and very low Sr/Y. These signatures along with high zircon saturation temperature indicate that these granites are derived from shallow partial melting of a tonalitic to granodioritic crust most probably the 3.55 Ga TTG crust. The occurrence of the A2 type Kuraicha granites is suggestive of an important (though poorly recognized) tectonothermal event in the later part of the Neoarchean-Paleoproterozoic granitoid magmatism in the BkC.

Acknowledgements: Authors thank the Chairperson, Department of Geology, AMU, Aligarh for providing necessary facilities to carry out the research work. Director, WIHG, Dehradun and Director, NGRI, Hyderabad are thanked for allowing us to carry out the geochemical analysis during the course of our study. Special thanks are due to Dr. M. Satyanarayanan who helped in the course of sample preparation and analysis. MMR acknowledges University Grants Commission, New Delhi for the award of Senior Research Fellowship (SRF) under the Basic Scientific Research (BSR) scheme, and to DST for the award of Junior Research Fellowship (JRF). Part of the research work has been financially supported by Department of Science and Technology (DST), Government of India, New Delhi, under a Major Research Project (SR/S4/ES-469/2009) sanctioned to MEAM. Dr. V. P. Malviya is thanked for his critical review which has helped in substantially improving an earlier version of the paper.

REFERENCES

Basu, A. K. (1986) Geology of parts of the Bundelkhand Granite Massif, Central India. Rec. Geol. Surv. India 117, pp. 61–124.

Barker, F. (1979) Trondhjemite: definition, environment and hypotheses of origin, *In:* Developments in Petrology. Elsevier, pp. 1–12. https://doi.org/10.1016/B978-0-444-41765-7.50006-X

Barker, F. and Arth, J.G. (1976) Generation of trondhjemitic-tonalitic liquids and Archean bimodal trondhjemite-basalt suites. Geology, v. 4, pp. 596-600. https://doi.org/10.1130/0091-7613(1976)4<596:GOTLAA>2.0.CO;2

Batuk Joshi, K., Bhattacharjee, J., Rai, G., Halla, J., Ahmad, T., Kurhila, M., Heilimo, E. and Choudhary, A.K. (2017) The diversification of granitoids and plate tectonic implications at the Archaean–Proterozoic boundary in the Bundelkhand Craton, Central India. Geol. Soc. Lond. Spec. Publ. 449, pp. 123–157. https://doi.org/10.1144/SP449.8

Bonin, B. (2007) A-type granites and related rocks: Evolution of a concept, problems and prospects. Lithos, v. 97, pp. 1–29. https://doi.org/10.1016/j.lithos.2006.12.007

Champion, D.C. and Sheraton, J.W. (1997) Geochemistry and Nd isotope systematics of Archaean granites of the Eastern Goldfields, Yilgarn Craton, Australia: implications for crustal growth

processes. Precambrian Res., v. 83, pp. 109–132. https://doi.org/10.1016/S0301-9268(97)00007-7

Creaser, R.A., Price, R.C. and Wormald, R.J. (1991) A-type granites revisited: Assessment of a residual-source model. Geology, v. 19, pp. 163. https://doi.org/10.1130/0091-7613(1991)019<0163:ATGRAO>2.3.CO;2

Du, L., Yang, C., Wyman, D.A., Nutman, A.P., Lu, Z., Song, H., Xie, H., Wan, Y., Zhao, L., Geng, Y. and Ren, L. (2016) 2090–2070Ma A-type granitoids in Zanhuang Complex: Further evidence on a Paleoproterozoic rift-related tectonic regime in the Trans-North China Orogen. Lithos, v. 254–255, pp. 18–35. https://doi.org/10.1016/j.lithos.2016.03.007

Eby, G. N. (1992) Chemical subdivision of the A-type granitoids: Petrogenetic and tectonic implications. Geology, v. 20, pp. 641. https://doi.org/10.1130/0091-7613(1992)020<0641:CSOTAT>2.3.CO;2

Frost, B.R., Barnes, C.G., Collins, W.J., Arculus, R.J., Ellis, D.J. and Frost, C.D. (2001) A geochemical classification for granitic rocks. J. Petrol., v. 42, pp. 2033–2048. https://doi.org/10.1093/petrology/42.11.2033

Frost, C.D. and Frost, B.R. (2011) On Ferroan (A-type) Granitoids: their Compositional Variability and Modes of Origin. J. Petrol., v. 52, pp. 39–53. https://doi.org/10.1093/petrology/egq070

Frost, C.D., Frost, B.R., Kirkwood, R. and Chamberlain, K.R. (2006) The tonalite–trondhjemite–granodiorite (TTG) to granodiorite–granite (GG) transition in the late Archean plutonic rocks of the central Wyoming Province. Can. J. Earth Sci., v. 43, pp. 1419–1444. https://doi.org/10.1139/e06-082

Gorring, M.L., Estelle, T.C. and Volkert, R.A. (2004) Geochemistry of the Late Mesoproterozoic Mount Eve granite suite: Implications for Late to post-Ottawan tectonics in the New Jersey-Hudson Highlands. Mem. Geol. Soc. Am. 197, pp. 505–524.

Guo, Z. and Wilson, M. (2012) The Himalayan leucogranites: Constraints on the nature of their crustal source region and geodynamic setting. Gondwana Res., v. 22, pp. 360–376. https://doi.org/10.1016/j.gr.2011.07.027

Harris, N., Ayres, M. and Massey, J. (1995) Geochemistry of granitic melts produced during the incongruent melting of muscovite: Implications for the extraction of Himalayan leucogranite magmas. J. Geophys. Res., v. 100, pp. 15767–15777. https://doi.org/10.1029/94JB02623

Hill, R.I. (1993) Mantle plumes and continental tectonics. Lithos, v. 30, pp. 193–206. https://doi.org/10.1016/0024-4937(93)90035-B

Inger, S. and Harris, N. (1993) Geochemical constraints on leucogranite magmatism in the Langtang Valley, Nepal Himalaya. J. Petrol., v. 34, pp. 345–368. https://doi.org/10.1093/petrology/34.2.345

Kaur, P., Zeh, A. and Chaudhri, N. (2014) Characterisation and U–Pb–Hf isotope record of the 3.55 Ga felsic crust from the Bundelkhand Craton, northern India. Precambrian Res., v. 255, pp. 236–244.

Kaur, P., Zeh, A., Chaudhri, N. and Eliyas, N. (2016) Unravelling the record of Archaean crustal evolution of the Bundelkhand Craton, northern India using U–Pb zircon–monazite ages, Lu–Hf isotope systematics, and whole-rock geochemistry of granitoids. Precambrian Res., v. 281, pp. 384–413. https://doi.org/10.1016/j.precamres.2016.06.005

King, P.L., Chappell, B.W., Allen, C.M. and White, A.J.R. (2001) Are A-type granites the high-temperature felsic granites? Evidence from fractionated granites of the Wangrah Suite. Aust. J. Earth Sci., v. 48, pp. 501–514. https://doi.org/10.1046/j.1440-0952.2001.00881.x

Lameyre, J. and Bowden, P. (1982) Plutonic rock types series: discrimination of various granitoid series and related rocks. J. Volcanol. Geotherm. Res., v. 14, pp. 169–186. https://doi.org/10.1016/0377-0273(82)90047-6

Laurent, O., Martin, H., Moyen, J.F. and Doucelance, R. (2014) The diversity and evolution of late-Archean granitoids: Evidence for the onset of “modern-style” plate tectonics between 3.0 and 2.5Ga. Lithos, v. 205, pp. 208–235. https://doi.org/10.1016/j.lithos.2014.06.012.

Malviya, V.P., Arima, M., Pati, J.K. and Kaneko, Y. (2006) Petrology and geochemistry of metamorphosed basaltic pillow lava and basaltic komatiite in Mauranipur area: subduction related volcanism in Archean Bundelkhand craton, Central India. Jour. Mineral. Petrol. Sci., v. 101, pp. 199-217.

Martin, H. and Moyen, J.-F. (2002) Secular changes in tonalite-trondhjemite-granodiorite composition as markers of the progressive cooling of Earth. Geology, v. 30, pp. 319. https://doi.org/10.1130/0091-7613(2002)030<0319:SCITTG>2.0.CO;2

Martin, H., Smithies, R.H., Rapp, R., Moyen, J.-F. and Champion, D. (2005) An overview of adakite, tonalite–trondhjemite–granodiorite (TTG), and sanukitoid: relationships and some implications for crustal evolution. Lithos, v. 79, pp. 1–24. https://doi.org/10.1016/j.lithos.2004.04.048

McDonough, W.F. and Sun, S.-S. (1995) The composition of the Earth. Chem. Geol., v. 120, pp. 223–253.

Mikkola, P., Huhma, H., Heilimo, E. and Whitehouse, M. (2011) Archean crustal evolution of the Suomussalmi district as part of the Kianta Complex, Karelia: Constraints from geochemistry and isotopes of granitoids. Lithos, v. 125, pp. 287–307. https://doi.org/10.1016/j.lithos.2011.02.012

Mohan, M.R., Singh, S.P., Santosh, M., Siddiqui, M.A. and Balaram, V. (2012) TTG suite from the Bundelkhand Craton, Central India: Geochemistry, petrogenesis and implications for Archean crustal evolution. J. Asian Earth Sci., v. 58, pp. 38–50.

Mondal, M.E.A. and S.M. Zainuddin (1997) Geochemical characteristics of the granites of Bundelkhand massif, central India. Jour. Geological Society of India, v. 50, pp. 69–74.

Mondal, M.E.A., Goswami, J.N., Deomurari, M.P. and Sharma, K.K. (2002) Ion microprobe 207 Pb/206 Pb ages of zircons from the Bundelkhand massif, northern India: implications for crustal evolution of the Bundelkhand–Aravalli protocontinent. Precambrian Res., v. 117, pp. 85–100.

Moyen, J. and Stevens, G. (2006) Experimental constraints on TTG petrogenesis: implications for Archean geodynamics. Archean Geodyn. Environ., v. 164, pp. 149–175.

Moyen, J.-F. (2011) The composite Archaean grey gneisses: Petrological significance, and evidence for a non-unique tectonic setting for Archaean crustal growth. Lithos, v. 123, pp. 21–36. https://doi.org/10.1016/j.lithos.2010.09.015

Moyen, J.-F., Champion, D. and Smithies, R. (2009) The geochemistry of Archaean plagioclase-rich granites as a marker of source enrichment and depth of melting. Earth Environ. Sci. Trans. R. Soc. Edinb., v. 100, pp. 35–50.

Moyen, J.-F. and Martin, H. (2012) Forty years of TTG research. Lithos, v. 148, pp. 312–336. https://doi.org/10.1016/j.lithos.2012.06.010

Moyen, J.-F., Martin, H., Jayananda, M. and Auvray, B. (2003) Late Archaean granites: a typology based on the Dharwar Craton (India). Precambrian Res., v. 127, pp. 103–123. https://doi.org/10.1016/S0301-9268(03)00183-9

O'connor, J. (1965) A classification for quartz-rich igneous rocks based on feldspar ratios. US Geol. Surv. Prof. Pap. B 525, pp. 79–84.

Pati, J.K., Patel, S.C., Pruseth, K.L., Malviya, V.P., Arima, M., Raju, S., Pati, P. and Prakash, K. (2007) Geology and geochemistry of giant quartz veins from the Bundelkhand Craton, central India and their implications. J. Earth Syst. Sci., v.116, pp. 497–510.

Pati, J.K., Reimold, W.U., Koeberl, C. and Pati, P. (2008) The Dhala structure, Bundelkhand Craton, Central India—Eroded remnant of a large Paleoproterozoic impact structure. Meteorit. Planet. Sci., v. 43, pp. 1383–1398.

Pearce, J.A., Harris, N.B.W. and Tindle, A.G. (1984) Trace element discrimination diagrams for the tectonic interpretation of granitic rocks. J. Petrol., v. 25, pp. 956–983. https://doi.org/10.1093/petrology/25.4.956

Pradhan, V.R., Meert, J.G., Pandit, M.K., Kamenov, G. and Mondal, M.E.A. (2012) Paleomagnetic and geochronological studies of the mafic dyke swarms of Bundelkhand Craton, central India: implications for the tectonic evolution and paleogeographic reconstructions. Precambrian Res., v. 198, pp. 51–76.

Ramiz, M.M. and Mondal, M.E.A. (2017) Petrogenesis of mafic magmatic enclaves of the Bundelkhand granitoids near Orchha, Central Indian shield: evidence for rapid crystallization. Geol. Soc. Lond. Spec. Publ. 449, pp. 159–173.

Ramiz, M.M., Mondal, M.E.A. and Farooq, S.H. (2018) Geochemistry of ultramafic–mafic rocks of the Madawara Ultramafic Complex in the southern part of the BundelkhandCraton, Central Indian Shield: Implications for mantle sources and geodynamic setting. Geological Journal,pp. 1–23, https://doi.org/10.1002/gj.3290

Rey, P.F., Philippot, P. and Thébaud, N. (2003) Contribution of mantle plumes, crustal thickening and greenstone blanketing to the 2.75–2.65Ga global crisis. Precambrian Res., v. 127, pp. 43–60. https://doi.org/10.1016/S0301-9268(03)00179-7

Rudnick, R.L. and Fountain, D.M. (1995) Nature and composition of the continental crust: A lower crustal perspective. Rev. Geophys., v. 33, pp. 267. https://doi.org/10.1029/95RG01302

Saha, L., Frei, D., Gerdes, A., Pati, J.K., Sarkar, S., Patole, V., Bhandari, A. and Nasipuri, P. (2016) Crustal geodynamics from the Archaean Bundelkhand Craton, India: constraints from zircon U–Pb–Hf isotope studies. Geol. Mag., v. 153, pp. 179–192.

Satyanarayanan, M., Balaram, V., Sawant, S., Subramanyam, K. and Krishna, G. (2014) High precision multielement analysis on geological samples by HR-ICPMS. Presented at the 28th ISMAS Symposium Cum Workshop on Mass Spectrometry. Indian Society For Mass Spectrometry, Mumbai, pp. 181–184.

Scaillet, B., Pichavant and M., Roux, J. (1995) Experimental crystallization of leucogranite magmas. J. Petrol., v. 36, pp. 663–705.

Shand, S.J. (1943) Eruptive rocks: their genesis, composition, classification, and their relation to ore-deposits with a chapter on meteorite, 2nd edition: New York, NY, John Wiley & Sons, 444 p.

Shirey, S.B. and Hanson, G.N. (1984) Mantle-derived Archaean monozodiorites and trachyandesites. Nature, v. 310, pp. 222–224. https://doi.org/10.1038/310222a0.

Singh, P.K., Verma, S.K., Singh, V.K., Moreno, J. A., Oliveira, E.P. and Mehta, P. (2019) Geochemistry and petrogenesis of sanukitoids and high-K anatectic granites from the Bundelkhand Craton, India: Implications for late-Archean crustal evolution. Journal of Asian Earth Sciences, v. 174, pp. 263-282.

Singh, S.P., Balaram, V., Satyanarayanan, M., Anjaiah, K.V. and Kharia, A. (2010) Platinum group elements in basic and ultrabasic rocks around Madawara, Bundelkhand Massif, Central India. Curr. Sci. 99, 375–383.

Singh, V.K. and Slabunov, A. (2015) The Central Bundelkhand Archaean greenstone complex, Bundelkhand Craton, central India: geology, composition, and geochronology of supracrustal rocks. Int. Geol. Rev., v. 57, pp. 1349–1364.

Singh, V. K., Verma, S. K., Singh, P. K., Slabunov, A. I., Mishra, S. and Chaudhary, N. (2019) Archean crustal evolution of the Bundelkhand Craton: Evidence from granitoid magmatism. Geological Society, London, Special Publications, v. 13, pp. 489.

Smithies, R.H. (2000) The Archaean high-Mg diorite suite: links to tonalite-trondhjemite-granodiorite magmatism and implications for early Archaean Crustal Growth. J. Petrol. 41, 1653–1671. https://doi.org/10.1093/petrology/41.12.1653

Streckeisen, A. (1976) To each plutonic rock its proper name. Earth-Sci. Rev., v. 12, pp. 1–33. https://doi.org/10.1016/0012-8252(76)90052-0

Sun, S. -S. and McDonough, W.F. (1989) Chemical and isotopic systematics of oceanic basalts: implications for mantle composition and processes. Geol. Soc. Lond. Spec. Publ., v. 42, pp. 313–345. https://doi.org/10.1144/GSL.SP.1989.042.01.19

Taylor, S. R. and McLennan, S. M. (1985) The continental crust: Its composition and evolution. xvi + 312 pp. Oxford, London, Geol. Mag., v. 122, pp. 673. https://doi.org/10.1017/S0016756800032167.

Topnoa, A., Dey, S., Liub, Y. and Zongb, K. (2018) Early Neoarchaean A-type granitic magmatism by crustal reworking in Singhbhum craton: evidence from Pala Lahara area, Orissa. J. Earth Syst. Sci., v. 127, pp. 1-22.

Verma, S.K., Verma, S.P., Oliveira, E.P., Singh, V.K. and Moreno, J.A. (2016) LA-SF-ICP-MS zircon U–Pb geochronology of granitic rocks from the central Bundelkhand greenstone complex, Bundelkhand Craton, India. J. Asian Earth Sci., v. 118, pp. 125–137.

Verma, S.K., Pandarinath, K., and Verma, S.P. (2012) Statistical evaluation of tectonomagmatic discrimination diagrams for granitic rocks and proposal of new discriminant-functionbased multi-dimensional diagrams for acid rocks: International Geology Review, v. 54, pp. 325–347. doi:10.1080/00206814.2010.543784

Verma, S. K., Verma, S. P., Oliveira, E. P., Singh, V. K. and Moreno, J. A. (2016) LA-SF-ICP-MS zircon U–Pb geochronology of granitic rocks from the central Bundelkhand greenstone complex, Bundelkhand craton, India. Journal of Asian Earth Sciences, v. 118, pp. 125-137.

Watson, E.B. and Harrison, T.M. (1983) Zircon saturation revisited: temperature and composition effects in a variety of crustal magma types. Earth Planet. Sci. Lett., v. 64, pp. 295–304. https://doi.org/10.1016/0012-821X(83)90211-X

Whalen, J.B., Currie, K.L., Chappell, B.W., 1987. A-type granites: geochemical characteristics, discrimination and petrogenesis. Contrib. Mineral. Petrol., v. 95, pp. 407–419. https://doi.org/10.1007/BF00402202

Table-1: Major elements (in wt%) and trace elements (in ppm) compositions of Kuraicha granites and gneiss of Bundelkhand Craton

	This study		Ramiz & Mondal, 2017		Kaur *et al.*, 2016	
Sample No.	KH449	KH450	MR150(G)	MR155(G)	BK-9	BK-7
GPS Location	N25°12.625 E79°06.087	N25°12.625 E79°06.087	N25° 13.098 E79° 10.528	N25° 12.589 E79° 06.089	N25°12.381 E79°06.540	N25°12.409 E79°06.006
SiO_2	76.7	76.7	77.2	79.2	74.3	74.4
TiO_2	0.09	0.07	0.05	0.08	0.19	0.09
Al_2O_3	12.8	13.2	12	11.2	13.3	15.0
$Fe_2O_3^t$	0.84	0.81	0.7	0.7	1.56	0.69
FeO^t	0.76	0.73	0.63	0.63	1.40	0.62
CaO	0.77	0.76	0.61	0.65	0.74	2.12
MgO	0.1	0.05	0.56	0.66	0.23	0.22
Na_2O	3.79	4.34	4.71	3.72	3.37	4.68
K_2O	4.74	4.54	4.96	4.9	5.34	2.79
MnO	0.02	0.04	0.03	0.02	0.03	0.01
P_2O_5	0.02	0.01	0.01	0.02	0.04	0.01
LOI	1.02	0.9	NA	NA	0.73	0.76
SUM	101.7	102.1	100.83	101.1	101.2	101.4
Sc	2.37	4.05	1.23	1.01	NA	NA
V	4.60	2.31	2.22	3.01	13	17
Cr	5.17	3.90	18.1	26.1	<20	<20
Co	50.7	40.4	17.6	20.8	25	28
Ni	9.00	7.30	3.33	6.03	<20	<20
Cu	7.92	2.13	0.50	9.55	NA	NA
Zn	56.8	19.0	1.45	1.61	40	40
Ga	23.5	23.6	21.4	17.2	21	19
Rb	430	513	494	429	349	88
Sr	41.6	16.4	13.4	28.6	66	466
Y	53.2	100	59.6	49.3	40	2
Zr	170	172	55.3	61.4	181	76
Nb	23.9	46.0	60.3	21.2	21	1
Cs	7.41	14.5	18.4	8.27	NA	NA
Ba	106	29.3	56.2	189	605	981
La	19.4	9.49	5.32	9.81	62.2	15.2
Ce	40.9	23.4	12.1	23.3	119	26.3
Pr	4.97	3.09	1.50	2.36	13.1	2.88
Nd	19.9	13.8	6.47	8.99	44.6	9.9
Sm	5.43	5.41	2.36	2.33	8.6	1.5
Eu	0.30	0.13	0.18	0.25	0.8	0.61
Gd	4.40	5.45	2.65	2.41	8.2	1
Tb	1.03	1.46	0.69	0.55	1.4	0.1
Dy	5.98	9.05	6.51	4.65	8.1	0.7
Ho	1.39	2.22	0.90	0.60	1.6	0.1
Er	4.51	7.61	3.79	2.37	4.5	0.3
Tm	0.76	1.35	0.63	0.37	0.68	0.05
Yb	6.42	11.5	7.34	4.12	4.3	0.3
Lu	1.21	2.23	1.34	0.70	0.6	0.06
Hf	9.87	11.9	3.31	3.07	6	2.6
Ta	6.89	12.0	6.15	3.79	2.7	0.2
Pb	23.8	24.4	34.0	31.8	44	13
Th	20.3	18.1	22.3	21.9	32.6	3.9
U	19.6	20.1	19.9	12.4	8.7	0.4
Na_2O+K_2O-CaO	7.8	8.1	9.1	8.0	7.97	5.35
FeO^t+MgO+MnO	0.88	0.82	1.22	1.31	1.66	0.85
Na_2O+K_2O	8.53	8.88	9.67	8.62	8.71	7.47
K_2O/Na_2O	1.25	1.05	1.05	1.32	1.58	0.60
(Na+K+2*Ca)/(Al*Si)	1.40	1.44	1.68	1.54	1.38	1.41
$(La/Yb)_{CN}$	2.06	0.56	0.49	1.62	9.83	34.4
$(La/Sm)_{CN}$	2.24	1.09	1.41	2.63	4.52	6.33
$(Gd/Yb)_{CN}$	0.55	0.38	0.29	0.47	1.54	2.70
Eu/Eu*	0.19	0.07	0.22	0.32	0.29	1.52
ΣREE	117	96.2	51.8	62.8	278	59
Ce/Pb	1.71	0.96	0.36	0.73	2.70	2.02

Nb/U	1.22	2.29	3.03	1.71	2.41	2.5
Rb/Sr	10.3	31.2	36.7	15.0	5.29	0.19
Sr/Y	0.78	0.16	0.23	0.58	1.65	233
ZST	792	789	684	699	799	724

$(La/Yb)_{CN}$, $(La/Sm)_{CN}$and $(Gd/Yb)_{CN}$ are ratio of chondrite-normalized elemental concentrations. $Eu/Eu^* = Eu/(Gd_{CN}*Sm_{CN})^{1/2}$. ZST - zircon saturation temperature (°C). NA: not available.

(Received: 04, 2020; Accepted: 25.10.2020)